Improved Constraints on an Axion-Mediated Force

S. A. Hoedl, F. Fleischer, E. G. Adelberger, and B. R. Heckel

Phys. Rev. Lett. **106**, 041801 — Published 24 January 2011

DOI: 10.1103/PhysRevLett.106.041801

Improved constraints on an axion-mediated force

S.A. Hoedl,* F. Fleischer, E.G. Adelberger, and B.R. Heckel

Center for Experimental Nuclear Physics and Astrophysics, Box 354290, University of Washington, Seattle, Washington 98195-4290, USA

Abstract

Low mass pseudo-scalars, such as the axion, can mediate macroscopic parity and time-reversal symmetry violating forces. We searched for such a force between polarized electrons and unpolarized atoms using a novel, magnetically unshielded torsion pendulum. We improved the laboratory bounds on this force by more than 10 orders of magnitude for pseudo-scalars heavier than 1 meV, and for the first time, have constrained this force over a broad range of astrophysically interesting masses (10 μeV to 10 meV).

PACS numbers: 14.80.Va

Low mass pseudo-scalars are predicted by string theories [1] and many extensions to the standard model. Such particles are typically associated with the spontaneous breaking of a new symmetry at a very high energy scale. The most well developed pseudo-scalar, the axion [2], is a consequence of Peccei and Quinn's solution to the "Strong-CP" problem: QCD explicitly violates the product of charge and parity (CP) reversal symmetry, so that the CP violating parameter, θ_{QCD}, is expected to be of order unity; however, bounds on the electric dipole moment of the neutron [3] and the Hg atom [4] constrain $\theta_{QCD} \leq 3 \times 10^{-10}$. To solve this fine-tuning problem, Peccei and Quinn proposed a new symmetry [5] that spontaneously broke in the very early Universe, dynamically minimized θ_{QCD} and generated the axion. Today, these axions would compose at least some of the cold dark matter [6].

Cosmology, astrophysics and laboratory experiments constrain the axion's mass and/or couplings. The present dark matter density imposes a model-dependent lower bound of about 10 μeV [7]. Estimations of stellar and supernovae energy loss rates impose an upper bound of about 10 meV [8]. Heavier axions that couple so strongly that they do not escape from stars or supernovae are precluded by laboratory-based particle physics experiments [9] and by limits on hot dark matter [10]. The constraints on the mass of pseudo-scalars other than axions must be evaluated for each model individually. Nevertheless, the axion mass bounds define an "axion-window" where most axion and pseudo-scalar search efforts are focused. In the remainder of this paper, we refer to both axions and similar pseudo-scalars as axion-like particle (ALPs).

Most ALP searches look for the conversion of a galactic [11], solar [12] or laboratory [13] origin ALP into a photon in the presence of a static magnetic field. However, any ALP that couples with both scalar and pseudo-scalar vertices to fundamental fermions would also mediate a parity and time-reversal symmetry violating (PTV) force [14] between a polarized electron and an unpolarized atom, described by the potential:

$$V(\hat{\sigma}, \boldsymbol{r}) = \frac{\hbar^2(\hat{\sigma} \cdot \hat{r})}{8\pi m_e} \left(\frac{g_s^a g_p^e}{\hbar c}\right) \left(\frac{1}{r\lambda_{\text{ALP}}} + \frac{1}{r^2}\right) e^{-r/\lambda_{\text{ALP}}} \tag{1}$$

where $\boldsymbol{r}$ is the electron-atom separation vector, $\lambda_{\text{ALP}} = m_{\text{ALP}}/\hbar c$ is the ALP Compton wavelength, $\hat{\sigma}$ and m_e are the spin unit-vector and mass of the polarized electron respectively. The ALP pseudo-scalar coupling constant to a polarized electron is g_p^e, and the ALP scalar coupling constant to an unpolarized atom is $g_s^a = Z(g_s^e + g_s^p) + N g_s^n$, where Z and N are the proton and neutron numbers respectively, and g_s^e, g_s^p and g_s^n are the scalar couplings to

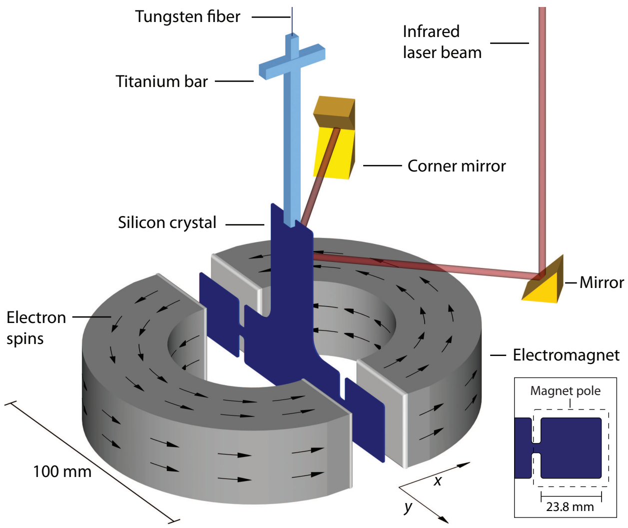

FIG. 1. (color online). A scale drawing of the torsion pendulum apparatus. The gap between the magnet halves, either 2.62 mm or 5.44 mm, is exaggerated for clarity. The inset shows the location of one cut-out in the silicon crystal with respect to the pole-face edges.

electrons, protons and neutrons respectively. For simplicity, we assume that $g_s^e = 0$ and that $g_s^p = g_s^n = g_s^N$, where g_s^N is the scalar coupling constant to a nucleon, so that $g_s^a = (Z+N)g_s^N$; the DFSZ [15] axion model, motivated by grand-unified theories, makes the same assumptions. Although $g_s^N g_p^e$ is expected to be very small (for the axion, $g_s^N \propto \theta_{QCD}$), PTV force searches have three advantages over more conventional ALP experiments: they do not rely on cosmological or astrophysical sources of ALPs; they are sensitive to ALPs that do not couple to photons, and most importantly, they can simultaneously probe the entire axion-window, which corresponds to a force with a range between 0.02 mm and 20.0 mm.

Previous PTV searches [16, 17] minimized background magnetic forces with magnetic shields that necessarily limited their sensitivity to a short-range PTV force. We overcame this limitation with an apparatus, shown in Fig. 1, that allowed us to observe an unshielded, highly non-magnetic torsion pendulum suspended by a tungsten fiber between two halves of a stationary split toroidal electromagnet. The pendulum consisted of semiconductor-grade silicon single-crystal attached to an ultra-pure titanium bar. An autocollimator monitored the pendulum's twist oscillation. The magnet-off pendulum period and Q were typically 280 s and 2500 respectively. The magnet-on Q was position dependent and ranged from 100 at $|x| = 1.2$ mm, to 1000 at $|x| = 0.0$ mm. A double layer mu-metal cylinder surrounded the magnet and reduced laboratory magnetic fields by a factor of 10^4.

A PTV force between the polarized electrons in the electromagnet and the unpolarized silicon atoms in the pendulum generates a magnetic-field-dependent (MFD) torque on the pendulum, given by $(g_s^N g_p^e/\hbar c)G(x, \lambda_{\rm ALP})B$, where $G(x, \lambda_{\rm ALP})$ is a geometrical factor calculated by integrating the PTV force over the polarized electrons in the magnet and the silicon atoms in the pendulum, x is the distance between the pendulum and the symmetry plane between the magnet halves, and B is the magnetic field in the gap between the magnet halves. The magnetic field generates two spurious MFD torques. First, frozen ferromagnetic impurities (FFIs) on the surface or in the bulk of the silicon create a MFD torque, given by $\mu_{\rm FFI}B$, where $\mu_{\rm FFI}$ is the fixed total magnetic moment perpendicular to the magnetic field and the fiber axis. Second, because silicon is diamagnetic, the pendulum seeks a rotation angle that minimizes the integral of B^2 over the pendulum's volume. The magnetic field, therefore, acted as a torsion spring, the "magnet spring," that was typically much stronger than the fiber spring itself. The magnet spring could mimic a MFD torque if its equilibrium angle were correlated with the magnetic field polarity.

Our pendulum design suppressed these spurious MFD torques. Metallic impurities in semi-conductor grade silicon are typically less than 1 ppb by atom [18]; they are also diffuse and unlikely to be FFIs because of the single-crystal nature of the material. We removed FFIs on the silicon surface by cleaning the pendulum according to the RCA1 and RCA2 protocols [19] that typically leave less than 10^{10} metal atoms per cm^2. The strength of the magnet spring was reduced by cut-outs in the silicon that minimized material in the magnetic field gradients at the pole-face edges (see inset of Fig. 1). A 300Å thick coating of paramagnetic terbium canceled the silicon's diamagnetism to within 5%. For a magnet gap of 5.44 mm, additional fine-tuning of the magnet spring was necessary and achieved by cooling the pendulum to 5°C (terbium's susceptibility is a strong function of temperature [20]).

The MFD torque was determined by observing the motion of the pendulum while repeatedly cycling between opposite magnet current states (Fig. 2a). For each magnet state, we monitored the pendulum's oscillation for an integral number of periods and then determined its equilibrium angle, oscillation amplitude, phase and period by a non-linear least squares fit. The data were divided into 12-cycle runs. The magnet spring equilibrium angles, $\theta_m^{\pm}$, and spring constants, $\kappa_m^{\pm}$, could differ in the clockwise (+) and counter-clockwise (−) magnet states. The observed equilibrium angles of the pendulum, $\theta^{\pm}$, must satisfy the equations:

$$\pm\bar{B}\left(\left(g_s^N g_p^e/\hbar c\right) G(x,\lambda_{\rm ALP}) + \mu_{\rm FFI}\right) \\ +\kappa_m^{\pm}\left(\theta^{\pm}-\theta_m^{\pm}\right) + \kappa_f\left(\theta^{\pm}-\theta_f\right) = 0, \quad (2)$$

where θ_f and κ_f are the equilibrium angle and spring constant of the fiber spring respectively, and $\bar{B}$ is the average absolute value of the magnetic field (measured with a Hall probe). We inferred the total spring constant, $\kappa^{\pm} = \kappa_f + \kappa_m^{\pm}$, from the pendulum period in each magnet state. Before and after each data run, we measured θ_f and κ_f. From Eq. 2, one can show that any MFD torque will generate a normalized torque asymmetry, defined as

$$\tilde{N} = \frac{1}{\bar{B}}\left[\bar{\kappa}\Delta\theta - \kappa_f \frac{\Delta\kappa(\bar{\theta}-\theta_f)}{\bar{\kappa}-\kappa_f}\right], \quad (3)$$

where $\Delta\theta = (\theta^+ - \theta^-)/2$ was determined using a filter that corrected for linear drift, $\bar{\theta} = (\theta^+ + \theta^-)/2$, $\Delta\kappa = (\kappa^+ - \kappa^-)/2$ and $\bar{\kappa} = (\kappa^+ + \kappa^-)/2$. The second term corrected for the spurious MFD torque created by a misalignment between the fiber and magnet-spring equilibrium angles. (The correction was typically smaller than the scatter among the cycles in each run). A PTV force, a FFI, and an asymmetry in the magnet spring equilibrium angle could all contribute to $\tilde{N}$ according to $\tilde{N} = \left(g_s^N g_p^e/\hbar c\right) G(x,\lambda_{\rm ALP}) + \mu_{\rm FFI} + \Delta\theta_m(\bar{\kappa}-\kappa_f)/\bar{B}$, where $\Delta\theta_m = (\theta_m^+ - \theta_m^-)/2$. Nevertheless, the PTV force has a unique signature: its finite range requires that $G(x,\lambda_{\rm ALP})$ must increase approximately as $\cosh(x/\lambda_{\rm ALP})$ as the pendulum approaches either magnet half. Because spurious MFDs should not exhibit this behavior (we test for this below), we could identify a true PTV force in the presence of spurious forces by measuring $\tilde{N}$ at different values of x.

We found that the pendulum's equilibrium angle depended on its horizontal position so that the autocollimator could only observe the pendulum when it was positioned on two lines in the horizontal plane (see inset, Fig. 2b). We measured $\tilde{N}$ at eight positions on these lines. Figure 2b plots a typical set of $\tilde{N}$s. Their position dependence was not consistent with a PTV force, but could be modeled by a function of the form $\tilde{N} = ax + by + c$, where x and y, defined in Fig. 1, were measured from the axial symmetry axis of the magnet halves, and $a \ll b$. At a fixed pendulum position, $\tilde{N}$ also depended on the history of the magnet. In particular, after demagnetizing the magnet by applying a linearly decreasing (9000 s decay time) harmonic current (36 s period), $\tilde{N}$ could change by up to ten times the 1-σ uncertainty expected given the scatter among the 12 cycles in each run. The demagnetization-induced changes in $\tilde{N}$ at different pendulum positions were correlated.

The demagnetization behavior and the linear y dependence can be explained by a degauss-dependent asymmetry in $\Delta\theta_m$. The magnet spring can be considered as two effective linear springs connected between the pendulum and the inner edge of each magnet pole-face. An asymmetry in the magnetic fields at the pole-face edges would create a difference in the equilibrium position of these linear springs in the two magnet states that would in turn create a $\Delta\theta_m$. Moving the pendulum along y changed the distance between the fiber axis and each linear spring. We expect $\Delta\theta_m$ to depend linearly on y for pendulum displacements that are small compared to the distance between the fiber axis and the pole-face edges. (The pendulum was translated by ± 1 mm along y while the fiber is 29 mm from the pole-face edge).

We constrained $g_s^N g_p^e/\hbar c$ in the presence of the demagnetization behavior and linear y dependence by segmenting the data-taking procedure into position scans, each of which consisted of a demagnetization, followed by measurements of $\tilde{N}$ at the different positions, and a subsequent fit of the linear model to this data. We repeated the position scan 20 times with fields of 0.387 T and 0.193 T and 2.62 mm magnet gap, and 23 times with a field of 0.109 T and a 5.44 mm magnet gap. The average of the residuals from each fit at a fixed x formed our ALP observable. Figure 2c shows the ALP observable as a function of x for the 2.62 mm gap data. The large-gap data extended our sensitivity to larger values of $\lambda_{\rm ALP}$ and also provided an important systematic check of the small gap data. The 1-σ error of the ALP observable (calculated from the scatter among the residuals in each data set) was dominated by the non-reproducible effects of the demagnetizing procedure (the thermal noise is a factor of 100 smaller). For a given $\lambda_{\rm ALP}$, we fit the predicted x-dependence of the PTV force to the ALP observables. (The predicted force conservatively accounted for the uncertainties in the pendulum's dimensions and relative position). The fits yielded larger than expected χ^2. To provide a 95% confidence limit, we inflated the ALP observable error bars for each fit so that $\chi^2/\nu = 1$, where ν is the number of degrees of freedom, and then found values of $g_s^N g_p^e$ so that $\Delta\chi^2 = 3.95$. The inflation factors were typically 2.50 and 2.08 for the 2.62 mm and 5.44 mm gap data respectively. We have no evidence for a PTV force. Figure 3 shows our exclusion bounds.

The $\mu_{\rm FFI}$ contribution is not expected to mimic a PTV force because $\bar{B}$ differs by less

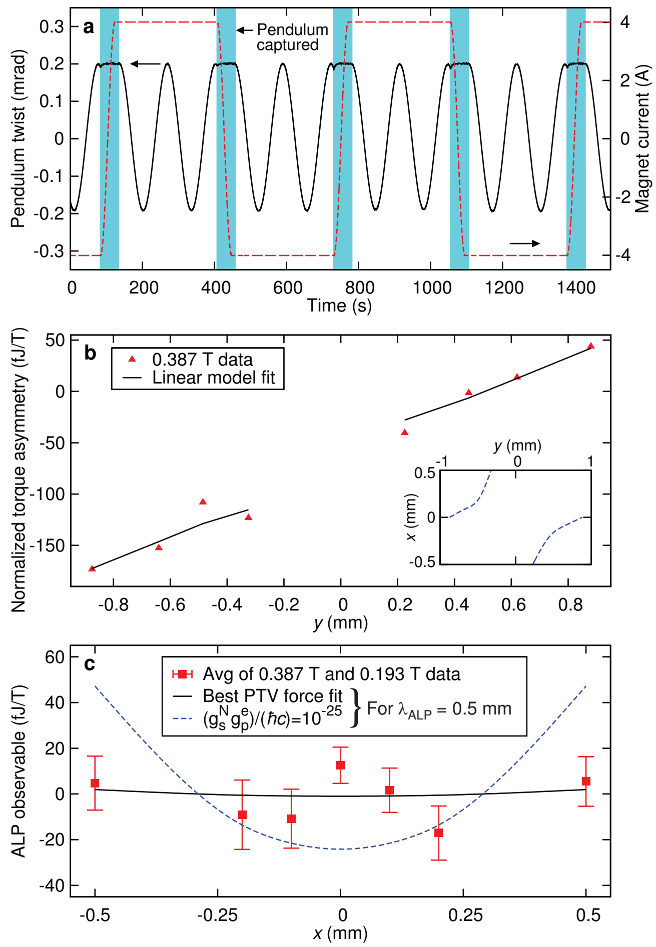

FIG. 2. (color online). (a) A typical interval of slightly more than two complete cycles of 0.193 T data. The shaded regions illustrate when an electrostatic feedback loop stabilized the pendulum. (b) Typical average $\tilde{N}$ data. The inset shows the positions where the autocollimator could observe the pendulum. (c) The ALP observables, best fit signal and a hypothetical PTV signal for the 2.62 mm gap data set.

than a few parts in 10^3 over the pendulum's positions. However, the $\Delta\theta_m$ contribution to $\tilde{N}$ could depend on the pendulum's x-position in a manner that mimicked a true PTV force signal and generated a systematic error. Because the pendulum's equilibrium angle depended on its location within the magnet halves, a x-dependent $\Delta\theta_m$ would occur if the tilt of the apparatus about the x or y-axis, the magnet temperature, or the absolute value of the magnetic field were correlated with the magnet state. (Because of the magnetic forces, the relative position of the magnet halves could depend on the absolute value of the magnetic field.) A laboratory magnetic field or field gradient that leaked through the magnetic shields

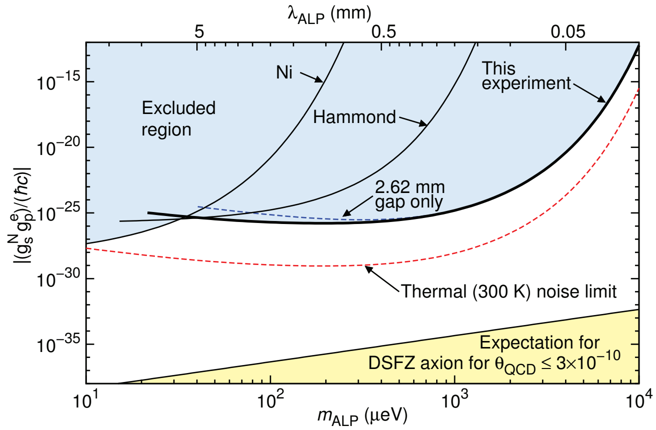

FIG. 3. (color online). The experimental 95% confidence upper limit on $|g_s^N g_p^e/\hbar c|$. The force mediated by the DFSZ [15] axion would appear below the bottom-most line. The thermal noise limit represents an ideal torsion pendulum with a magnet-on Q of 3000. See Ref. [21] for bounds on the PTV force between polarized and unpolarized nucleons.

would also create a $\Delta\theta_m$ that could depend on the pendulum position.

For each of these systematic errors, we modified the experiment to exaggerate the effect, measured $\tilde{N}$ at eight pendulum positions and solved for a PTV force using the same method employed to analyze the ALP observable. The systematic error corrections listed in Table 1 were calculated by multiplying $g_s^N g_p^e/\hbar c$, extracted from the exaggerated data, by the ratio of the normal to the exaggerated effects. The total systematic error was less than its 1-σ uncertainty, which itself was a factor of thirty smaller than the bound on $g_s^N g_p^e/\hbar c$ for all $\lambda_{\rm ALP}$ so that corrections to the statistical confidence bounds plotted in Fig. 3 were not required.

We have substantially improved the bounds on a PTV force between polarized electrons and unpolarized nucleons over most of the axion-window, tightening existing constraints on ALPs heavier than 1 meV by more than a factor of 10^{10}. Our experimental sensitivity was limited by demagnetization scatter and by deviations from a simple model of the linear position dependence of the normalized torque asymmetry. We hypothesize that slight asymmetries in the magnetic field at the pole-face edges generated both effects. Further improvement could be achieved by constructing a magnet from a laminated ferromagnetic material that generates a more homogeneous and reproducible magnetic field profile and by using a pendulum constructed of a denser material such as germanium. Such an experiment would more closely approach the thermal limit and could ultimately yield constraints

TABLE I. Systematic error summary for the 2.62 mm gap data. The systematic errors for the 5.44 mm gap data are less than those listed here. The uncertainties for other values of λ_{ALP} scale with the statistical sensitivity plotted in Fig. 3.

Systematic error	Size of effect	Correction to $g_s^N g_p^e/\hbar c$ for $\lambda_{\text{ALP}} = 0.5$ mm
y-axis tilt	$+2.20 \pm$ 3.30 nrad	$(+4.60 \pm 6.90) \times 10^{-28}$
x-axis tilt	$-0.10 \pm$ 1.60 nrad	$(-0.23 \pm 3.68) \times 10^{-28}$
$\|B\|$	$+7.0 \pm$ 0.8 μT	$(0.00 \pm 1.96) \times 10^{-28}$
Magnet Tem.	$-0.32 \pm$ 0.27 mK	$(-9.63 \pm 9.49) \times 10^{-29}$
Lab. B_y	$+27 \pm$ 1 μT	$(+1.46 \pm 1.29) \times 10^{-29}$
Lab. ∇B_x	$+3.7 \pm$ 0.8 μT/mm	$(-2.55 \pm 9.68) \times 10^{-30}$
Lab. B_x	$+23 \pm$ 2 μT	$(+0.74 \pm 7.77) \times 10^{-29}$
Lab. ∇B_y	$+0.6 \pm$ 0.6 μT/mm	$(-1.05 \pm 1.82) \times 10^{-30}$
Total		$(+3.51 \pm 8.12) \times 10^{-28}$

a factor of 1000 better than those presented here.

This work was supported by the US National Science Foundation through grant NSF-PHY0653863 and by the US Department of Energy funding for the CENPA laboratory at the University of Washington. F.F. thanks the Alexander von Humboldt Foundation for support as a Feodor Lynen Fellow. We thank H. Simons for his instrument-making expertise, and L. Rosenberg and A. Young for their comments on the manuscript.

* sethh@uw.edu

[1] P. Svrcek and E. Witten, JHEP, **0606**, 051 (2006).

[2] S. Weinberg, Phys. Rev. Lett., **40**, 223 (1978); F. Wilczek, *ibid.*, **40**, 279 (1978).

[3] C. Baker *et al.*, Phys. Rev. Lett., **97**, 131801 (2006).

[4] W. Griffith *et al.*, Phys. Rev. Lett., **102**, 101601 (2009).

[5] R. Peccei and H. Quinn, Phys. Rev. D, **16**, 1791 (1977).

[6] S. Asztalos *et al.*, Ann. Rev. Nucl. Part. Sci., **56**, 293 (2006).

[7] S. Asztalos *et al.*, Phys. Rev. D, **69**, 011101(R) (2004).

[8] G. Raffelt, Ann. Rev. Nucl. Part. Sci., **49**, 163 (1999).

[9] J. Kim, Physics Reports, **150**, 1 (1987).

[10] S. Hannestad *et al.*, JCAP, **08**, 1 (2010).

[11] S. Asztalos *et al.*, Phys. Rev. Lett., **104**, 041301 (2010).

[12] E. Arik *et al.*, JCAP, **02**, 008 (2009).

[13] K. Ehert *et al.*, Phys. Lett. B, **689**, 149 (2010).

[14] J. Moody and F. Wilczek, Phys. Rev. D, **30**, 130 (1984).

[15] M. Dine *et al.*, Phys. Lett. B, **104**, 199 (1981); A. Zhitnitskii, Sov. J. Nucl. Phys., **31**, 260 (1980).

[16] W.-T. Ni *et al.*, Phys. Rev. Lett., **82**, 2439 (1999).

[17] G. Hammond *et al.*, Phys. Rev. Lett., **98**, 081101 (2007).

[18] L. Rogers, in *Handbook of Semiconductor Silicon Technology*, edited by W. O'Mara *et al.* (Noyes, 1990) p. 85.

[19] D. Burkman *et al.*, in *Handbook of Semiconductor Wafer Cleaning Technology – Science Technology and Applications*, edited by W. Kern (Noyes, 1993).

[20] J. Rhyne, in *Magnetic Properties of Rare Earth Metals*, edited by R. Elliott (Plenum, 1972) p. 132.

[21] S. Baessler *et al.*, Phys. Rev. D, **75**, 075006 (2007); A. Petukhov *et al.*, Phys. Rev. Lett., **105**, 170401 (2010).